fire

MDPI

Article

Exploring the Application Potential and Performance of SiO_2 Aerogel Mortar in Various Tunnel High-Temperature Environments

Hongyun Chen [1], Pinghua Zhu [2,*], Xiancui Yan [2], Xiaoyan Xu [2] and Xinjie Wang [2]

[1] School of Environmental Science and Engineering, Changzhou University, Changzhou 213164, China; chenhongyun0330@163.com
[2] School of Urban Construction, Changzhou University, Changzhou 213164, China; yanxc@cczu.edu.cn (X.Y.); xuxiaoyancczu@163.com (X.X.); wangxinjie@cczu.edu.cn (X.W.)
* Correspondence: zph@cczu.edu.cn

Abstract: SiO_2 aerogel is a super-insulating material that can be used for tunnel fireproofing to eliminate high-temperature spalling and extend the safe evacuation time of personnel. This study aimed to replace traditional aggregates with SiO_2 aerogel in mortar preparation and evaluate its mechanical properties, thermal conductivity, and durability (freeze–thaw, water, and moisture resistance). Furthermore, the high-temperature characteristics of SiO_2 aerogel and the damage evolution pattern of SiO_2 aerogel mortar were investigated with varying fire durations (0.5, 1, 1.5, 2, 2.5, and 3 h) and fire temperatures (1000, 1100, and 1200 °C) as environmental variables. The results revealed that the critical temperature and critical time of SiO_2 aerogel particles from amorphous to crystalline structures were about 1100 °C and 1.5 h, respectively. SiO_2 aerogel mortar exhibited a compressive strength of 3.5 MPa, a bond strength of 0.36 MPa, and a thermal conductivity of 0.165 W/m·K. The residual mass ratio and residual compressive strength of SiO_2 aerogel mortar were 81% and 1.8 MPa after 1100 °C for 2.5 h. The incorporation of SiO_2 aerogel significantly improved the fire resistance of the mortar. Therefore, SiO_2 aerogel mortar has the potential to be used as a fireproof coating and can be applied in tunnels to reduce high-temperature spalling and extend the safe evacuation time for personnel.

Keywords: aerogel high-temperature characteristics; tunnel fires; SiO_2 aerogel mortar; thermal damage

Citation: Chen, H.; Zhu, P.; Yan, X.; Xu, X.; Wang, X. Exploring the Application Potential and Performance of SiO_2 Aerogel Mortar in Various Tunnel High-Temperature Environments. *Fire* **2023**, *6*, 407. https://doi.org/10.3390/fire6100407

Academic Editor: Grant Williamson

Received: 12 September 2023
Revised: 11 October 2023
Accepted: 17 October 2023
Published: 20 October 2023

1. Introduction

Urbanization has driven the extensive utilization of subterranean urban spaces and facilitated rapid urban transportation. The proliferation of railway tunnels, including underground road tunnels and subway tunnels, has effectively alleviated traffic pressures compared to traditional road networks. However, it is essential to acknowledge that tunnel networks pose a higher potential risk in the event of traffic accidents [1–3]. Tunnels are enclosed cylindrical structures with narrow spaces. Smoke and heat are difficult to disperse in tunnels, which imposes restrictions on firefighting and rescue operations and exacerbates the escape difficulty for trapped individuals. Tunnel fires, such as truck or tanker accidents, can reach 1000 °C within 10 min, which are extremely difficult to extinguish [4]. The fire accident will cause casualties, damage tunnel facilities, impact society profoundly, and result in property losses [5–9]. Consequently, the safety problems caused by tunnel fires have attracted wide attention from the academic community and have become a pivotal research focus in contemporary society.

Until now, researchers have made considerable efforts to enhance the fire resistance of concrete structures [10–15]. In these studies, fireproof coatings have been applied on tunnel concrete surfaces as an effective method to mitigate concrete spalling issues during tunnel fires. However, certain organic coatings, including polyurethane foams, present a drawback

due to the substantial release of toxic gases at elevated temperatures during fires. These emissions pose the risk of environmental pollution and human poisoning. Many scholars considered the use of low thermal conductivity aggregates as a convenient approach in the production of cement mortar coatings. Koksal et al. [16] discovered that using expanded vermiculite and calcium aluminate cement enables the preparation of fire-resistant mortar with excellent refractoriness at temperatures as high as 900 °C. Huang et al. [17] achieved compressive strengths of 32.8% to 45.6% of the initial strength in mortar made from alkali-activated slag-crushed aggregates during a 900 °C fire. Ding et al. [18] also developed a refractory and insulating composite material using expanded perlite as the aggregate. Krivenko et al. [19] successfully prepared a high-performance alkali-aluminosilicate fire-proof coating, which can effectively resist fire at 1100 °C for 2 h. Wang et al. [10] developed a fireproof coating with superior fire insulation capabilities, effectively preventing high-temperature bursting and spalling of concrete during a 90 min fire exposure. However, there remains a relative scarcity of research on fireproof coatings with prolonged resistance to tunnel fires.

Aerogel particles have lightweight, porous, super-adiabatic characteristics, and easy functionalization, which means that this material has great potential in thermal insulation. The utilization of the sol–gel process, aging technique, and supercritical drying enables the synthesis of an aerogel with exceptionally low thermal conductivity [20]. Incorporating aerogel into cementitious materials demonstrates a pronounced reduction in the thermal conductivity of composites, offering great possibility for building energy conservation [21–24]. Zhang et al. [25] developed a multifunctional cementitious composite by incorporating aerogel as a lightweight aggregate. When 20% of the sand was replaced with aerogel, the material exhibited a thermal conductivity of 0.31 W/m·K. Lu et al. [26] successfully prepared a composite material with a density of 390 kg/m^3 and a thermal conductivity of 0.067 W/m·K by replacing 66% of the cement paste volume with aerogel. The thermal insulation performance of aerogel as a porous material mainly depends on the size of the pores [27]. Under continuous ultra-high-temperature conditions, a SiO_2 aerogel underwent structural collapse, resulting in volume shrinkage and increased thermal conductivity, which affected its insulating capability [28–30]. Previous studies mainly focused on incorporating the SiO_2 aerogel to reduce the thermal conductivity of cement mortar, thereby reducing the energy consumption of structures. Notably, the current studies on the characteristics of aerogel at high temperatures remain inadequate, and the research concerning the application of aerogel cement mortar under tunnel fire conditions is still relatively limited.

This study investigated the high-temperature characteristics of the SiO_2 aerogel under different fire temperatures (1000–1200 °C) and durations (0–3 h). Additionally, the damage to the prepared SiO_2 aerogel mortar was assessed. The macroscopic performance damage of the SiO_2 aerogel mortar was assessed through changes in morphology, mass loss rate, and residual compressive strength. Scanning Electron Microscopy (SEM) was utilized to examine the microstructural degradation induced by high temperatures. X-ray Diffraction (XRD) analysis was employed to evaluate the phase transition of SiO_2 aerogel mortar and SiO_2 aerogel at various durations during various fire temperatures. The outcome culminated in successfully developing an environmentally friendly, high-temperature resistant, and durable fireproof mortar.

2. Materials and Methods

2.1. Materials

P.O 42.5 ordinary Portland cement was used. The mineral admixtures were silica fume (SF) and fly ash (FA). The chemical compositions of the cementitious materials are listed in Table 1. Polycarboxylic acid high-performance water-reducing agent (WRA) with a 30% water reduction rate and an air entraining agent (AEA) with a 4% air content were used as admixtures. The commercial hydrophobic SiO_2 aerogel was chosen to conduct

high-temperature tunnel fire tests and substitute traditional aggregates to prepare SiO_2 aerogel mortar. The basic properties of SiO_2 aerogel mortar are listed in Table 2.

Table 1. Chemical compositions of cementitious materials (wt%).

Compositions	SiO_2	Al_2O_3	Fe_2O_3	TiO_2	CaO	MgO	K_2O	Na_2O	Others
Cement	21.55	4.39	3.37	0.61	63.68	1.22	0.89	0.30	3.98
FA	37.87	24.82	10.89	2.01	14.79	0.99	2.01	0.58	6.04
SF	95.2	0.05	-	-	1.21	0.08	0.01	-	3.45

Table 2. Fundamental properties of SiO_2 aerogel.

Particle Size (mm)	Surface Properties	Density (kg/m^3)	Aperture (nm)	Specific Surface Area (g/m^2)	Thermal Conductivity (W/m·K)	Porosity (%)
3	Hydrophobic	100	20–100	788	0.020	>90

2.2. Mix Proportion

In this experiment, the wet density of SiO_2 aerogel mortar was designed to be 700 kg/m^3. According to the optimal slurry–bone ratio, the amount of cementitious material was designed to be 450 kg/m^3. FA and SF accounted for 20% and 10% of the cementitious materials by mass, respectively. The water–binder ratio was 0.4. The amount of aerogel was calculated using the volume method specified in GB/T20473-2021 [31]. The WRA and AEA were incorporated at 1% and 0.8% of the cementitious materials mass, respectively. Table 3 shows the specific mix proportions.

Table 3. Mix proportions of SiO_2 aerogel mortar (kg/m^3).

No.	Aerogel	Sand	Cement	Water	FA	SF	WRA	AEA
AM0	0	1722.5	315	180	90	45	4.5	3.6
AM1	65	0	315	180	90	45	4.5	3.6

2.3. Specimen Preparation

Initially, the cementitious materials, AEA, WRA, and half of the water were blended and stirred for 60 s. Subsequently, the SiO_2 aerogel was added to the mixture, followed by the addition of the remaining water. The mixture was then stirred for an additional 120 s to ensure proper integration. After the mixing was completed, the SiO_2 aerogel mortar was poured into steel molds and solidified for 24 h before demolding. The standard was carried out for 28 d afterward.

2.4. Test Methods

The compressive strength was determined according to the GB28375-2012 [32]. After standard curing, the 70.7 mm × 70.7 mm × 70.7 mm specimens were uniformly loaded at 150 N/min until the specimens were destroyed, and three specimens were taken for testing.

The bond strength was evaluated according to the JGJ/T70-2009 [33]. A 40 mm × 40 mm × 3 mm SiO_2 aerogel mortar specimen was applied to a cement mortar substrate measuring 70 mm × 70 mm × 20 mm. After being cured under standard conditions for 28 d, the specimens were subjected to failure loading at a 5 mm/min rate. A total of three specimens were tested.

According to GB28375-2012 [32], the specimens (150 mm × 70 mm × 10 mm) were tested for water, moisture, and freeze–thaw resistance. In the water resistance test, three specimens were immersed in tap water with their short edges facing down, and the immersion depth was 2/3 of their long edges and observed every 24 h. In the moisture resistance test, the specimens were positioned within a test chamber with humidity (90 ± 5%) and

temperature (45 ± 5 °C). They were observed every 24 h. In the freeze–thaw resistance test, the specimens were initially placed in a low-temperature chamber at (−20 ± 2 °C) for 3 h and then immediately transferred to a constant temperature chamber at (50 ± 2 °C) for 3 h, constituting one cycle. Observations were made at the end of each freeze–thaw cycle.

The thermal conductivity was tested following GB/T10294-2008 [34]. The specimens' dimensions were 300 mm × 300 mm × 30 mm.

To simulate tunnel fire conditions and investigate the thermal damage mechanisms of SiO_2 aerogel and the developed SiO_2 aerogel mortar at different durations of tunnel fires, peak temperatures of 1000, 1100, and 1200 °C were, respectively, set. The rates of temperature rise and fall were 30 °C/min and 10 °C/min, respectively. The SiO_2 aerogel and SiO_2 aerogel mortar were exposed to high temperatures for durations of 0.5, 1, 1.5, 2, 2.5, and 3 h. After the fire experiments, the SiO_2 aerogel mortar was subjected to mass and compressive strength measurements to determine residual mass fraction and residual compressive strength.

This experiment examined the chemical composition of cementitious materials using APEXII X-ray single-crystal diffraction. The microstructures of SiO_2 aerogel and SiO_2 aerogel mortar after exposure to different time–temperature tunnel fire conditions were investigated utilizing a SUPRA55 scanning electron microscope. The phase structure of SiO_2 aerogel and SiO_2 aerogel mortar was analyzed using D/MAX2500X-ray powder diffractometer. Through microscopic analysis, the thermal damage mechanism under tunnel fire was revealed.

3. Results and Discussion

3.1. Morphology of SiO_2 Aerogel after Tunnel Fire

The morphology changes of SiO_2 aerogel after tunnel fires at different temperatures and durations are shown in Figure 1. Before the fire, the SiO_2 aerogel appeared as translucent particles. After 3 h of fire at 1000 °C (Figure 1a), its apparent morphology did not change significantly under the high-temperature environment. It still showed light-blue translucent particles with no noticeable volume shrinkage. Indicating that high temperature did not damage its nanoporous network structure. After the fire temperature reached 1100 °C (Figure 1b), the aerogel particles gradually changed from light-blue translucent particles to milky-white opaque particles after 0.5–1 h of sustained high temperature. However, no apparent shrinkage occurred. As the fire time prolonged, the aerogel particles gradually changed from translucent to milky-white and underwent severe volume shrinkage. After 1.5 h, the aerogel particles had shrunk noticeably, in line with the findings of Huang et al. [28]. When the fire temperature reached 1200 °C (Figure 1c), the aerogel particles became hard transparent crystals and shrank violently after heating for 0.5 h., and severe shrinkage occurred. The fire insulation ability of the SiO_2 aerogel mainly comes from its nanoporous network structure [35,36], but a continuous high temperature destroys its network structure and significantly reduces its fire insulation ability [28,29]. In order to prevent the structural damage of the aerogel at high temperatures and improve its fire insulation capability, researchers recommend combining it with other materials.

3.2. SEM Analysis of SiO_2 Aerogel

The morphological changes of the SiO_2 aerogel after being exposed to different durations of tunnel fire were shown in Figure 2. The microscopic structure of SiO_2 aerogel particles is a three-dimensional nanoporous structure characterized by a loose arrangement [37,38]. The SiO_2 aerogel was translucent before the fire, and its microstructure did not change much under 3 h of high temperature at 1000 °C. It still remained loose and translucent, and its porous structure did not undergo any obvious change, which is consistent with its macroscopic morphology (Figure 1a). However, after 0.5–3 h of fire at 1100 °C, many white particles emerged on the surface of the aerogel, making it rougher. This was caused by the surface collapse of the aerogel structure under the high fire temperature. As the heating time exceeded 1.5 h, the aerogel particles shrank considerably

in volume, showing an opaque morphology. As time passed, the aerogel contracted further, and its surface gradually smoothed out, but it remained rough after 3 h of high fire temperature. When the fire temperature reached 1200 °C, the aerogel particles turned into transparent crystal-like structures after 0.5 h of fire, and their volume reduced drastically. With the extension of the fire time, their volume hardly changed, indicating that the aerogel particles had virtually no resistance under the high fire temperature of 1200 °C.

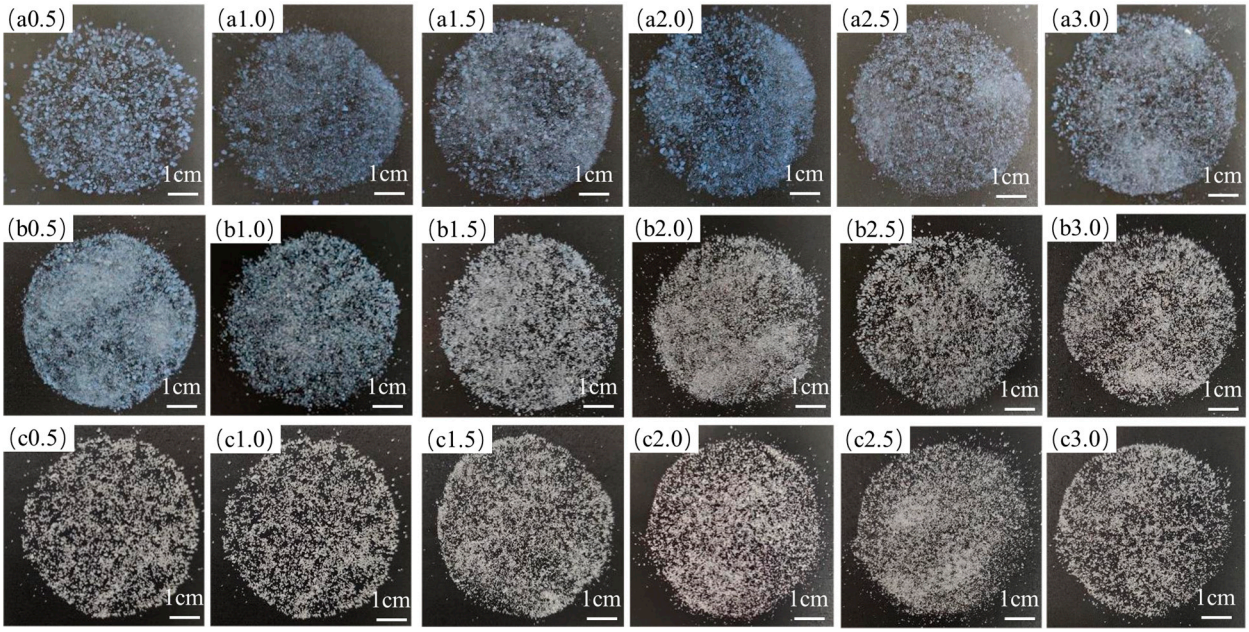

Figure 1. Macroscopic morphology of SiO_2 aerogel particles exposed to different temperatures and durations: (**a**) 1000 °C; (**b**) 1100 °C; (**c**) 1200 °C.

3.3. XRD Analysis of SiO_2 Aerogel

The XRD patterns of the SiO_2 aerogel exposed to various fire temperatures and durations are shown in Figure 3. The diffraction peak appeared near $2\theta = 23°$, corresponding to amorphous SiO_2 [39]. According to the XRD results, the SiO_2 aerogel did not show crystalline diffraction peaks when exposed to 1000 °C, which meant that the SiO_2 aerogel could remain in an amorphous state when the fire temperature was less than or equal to 1000 °C. This corresponded to the microscopic results shown in Figure 2a. When exposed to a temperature of 1100 °C, the SiO_2 aerogel retained its amorphous structure after burning for 0.5 to 1 h. The half-peak width of the diffraction envelope peak at $2\theta = 23°$ gradually decreased as the fire duration increased. When the burning time exceeded 1.5 h, the diffraction peak at $2\theta = 26.5°$ corresponded to the SiO_2 crystal [40]. The SiO_2 aerogel underwent a phase transition from an amorphous to a crystalline structure, indicating that the silica's silicon–oxygen tetrahedra could rearrange themselves and form an ordered crystal structure under sufficiently high temperatures. Researchers have reported that the amorphous SiO_2 aerogel transformed into a crystalline SiO_2 structure at temperatures above 1100 °C [41], which agreed with our experimental observations. At 1200 °C, the SiO_2 aerogel began to crystallize after 0.5 h of exposure to fire, and its crystallinity increased with longer fire duration, which further explained the changes in its microstructure (Figure 2c). Based on the results of this study and previous studies, the SiO_2 aerogel maintained its amorphous structure and high-temperature resistance at temperatures below 1000 °C. The critical temperature and time for the SiO_2 aerogel to transform from amorphous to crystalline were approximately 1100 °C and 1.5 h, respectively. At 1200 °C, the SiO_2 aerogel was prone to structural changes.

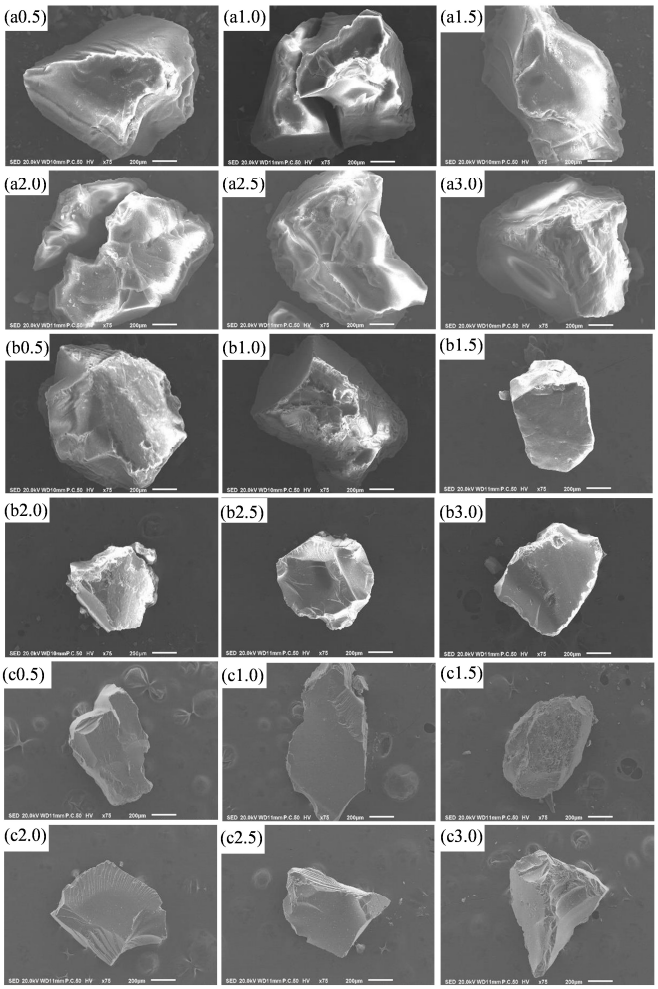

Figure 2. SEM images of SiO_2 aerogel particles exposed to different fire temperatures and durations: (**a**) 1000 °C; (**b**) 1100 °C; (**c**) 1200 °C.

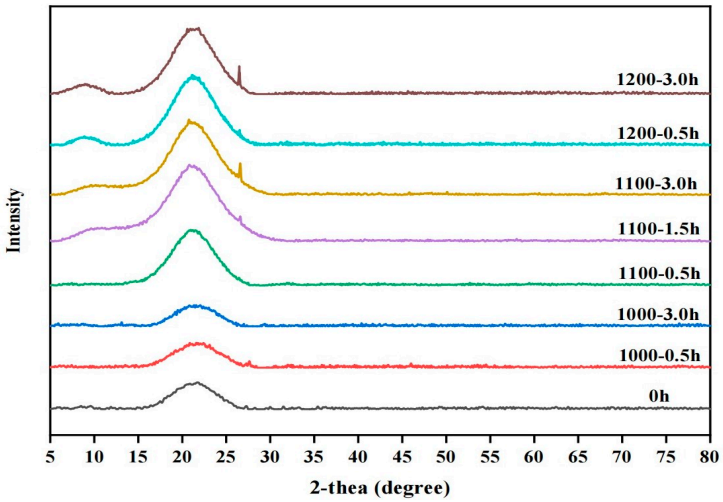

Figure 3. XRD patterns of SiO_2 aerogel particles after exposure to different fire temperatures and durations.

3.4. Properties of SiO_2 Aerogel Mortar

Table 4 showed the basic properties of SiO_2 aerogel mortar. The thermal conductivity of SiO_2 aerogel mortar was only 0.165 W/m·K, about 20% of that of conventional

cement mortar. By replacing the fine aggregate in the conventional mortar with SiO_2 aerogel, the thermal conductivity of the mortar was significantly reduced, enhancing its thermal insulation performance. The pozzolanic reaction between silica fume and fly ash and $Ca(OH)_2$ generated by the hydration process of cement produced a large amount of C-S-H gel. This resulted in a more uniform and denser microstructure, contributing to the enhancement of the material strength and durability. Since the thermal stability of C-S-H was higher than that of Ca $(OH)_2$, the material's fire resistance was also improved. Furthermore, the SiO_2 aerogel, due to its high surface area, is susceptible to reacting with a pore solution, leading to its structural collapse. The pozzolanic reaction of silica fume and fly ash better protects the SiO_2 aerogel, allowing it to remain stable in the cement pore solution environment [42]. The compressive strength, bond strength, dry density, water resistance, moisture resistance, and freeze–thaw resistance of the SiO_2 aerogel mortar met the requirements of GB 28375-2012 [32]. All the test indexes proved that the SiO_2 aerogel mortar has the potential to become a fireproof coating.

Table 4. Performance of SiO_2 Aerogel Mortar.

	Compressive Strength (MPa)	Bond Strength (MPa)	Dry Density (kg/m^3)	Water Resistance (h)	Moisture Resistance (h)	Freeze–Thaw Resistance (times)	Thermal Conductivity (W/m·K)
AM0	22	2.4	1950	≥720	≥720	≥15	1.32
AM1	3.5	0.36	658	≥720	≥720	≥15	0.165
Standard Values	≥1.5	≥0.15	≤700	≥720	≥720	≥15	

3.5. Morphology of SiO_2 Aerogel Mortar after Tunnel Fire

The SiO_2 aerogel mortar showed different characteristics in its apparent morphology after exposure to different temperatures and durations of fire, as shown in Figure 4. The thermal damage of cement-based materials mainly included high-temperature discoloration, cracking, and spalling [43,44].

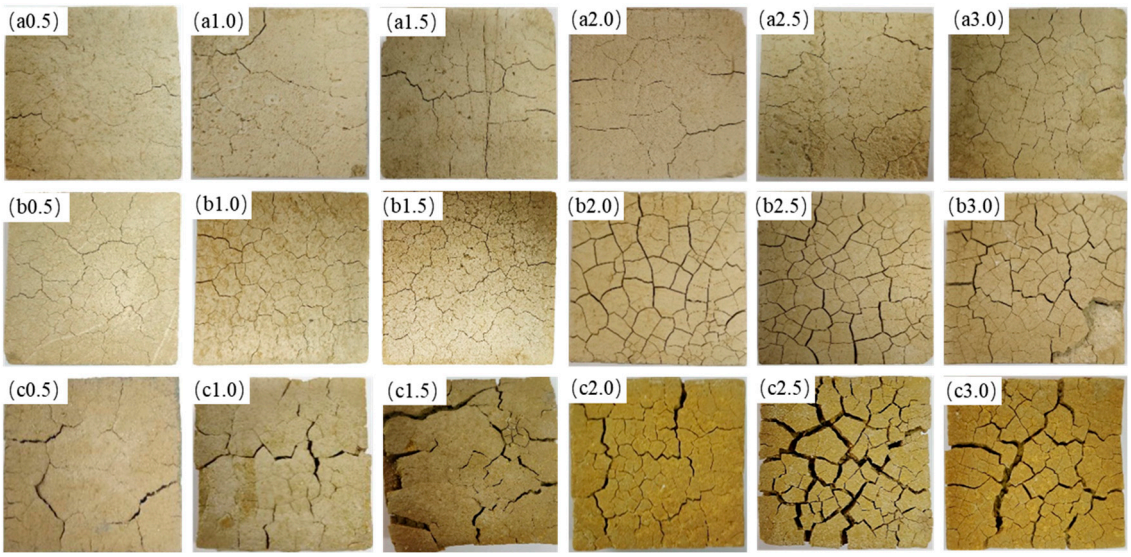

Figure 4. Morphology of SiO_2 aerogel mortar after exposure to different fire temperatures and durations: (**a**) 1000 °C; (**b**) 1100 °C; (**c**) 1200 °C.

The SiO_2 aerogel mortar was gray-white before the fire and had a dense structure with tight bonding between the mortar and the aerogel particles. The hydrophobic SiO_2 aerogel particles can exist stably in the cement slurry. After exposure to different temperatures and durations of fire, the SiO_2 aerogel mortar did not exhibit large-scale spalling and showed

high stability. Under the high-temperature conditions of 1000–1100 °C, the SiO_2 aerogel mortar did not undergo apparent volume shrinkage, but the surface became looser due to the high temperature. However, the SiO_2 aerogel mortar underwent significant shrinkage and the surface hardened at 1200 °C.

Cracking occurred in the SiO_2 aerogel mortar after fire exposure. When the fire temperature was 1000–1100 °C, the crack development of SiO_2 aerogel mortar showed a stable trend between 0.5 h and 1 h, with minor damage. However, as the fire duration exceeded 1.5 h, the crack development intensified, and the damage further expanded. When the fire temperature reached 1200 °C, the crack development gradually increased without a stable stage. The SiO_2 aerogel mortar prepared in this experiment maintained high volume stability under fire temperatures below 1100 °C, although it had cracks, which proved that it had certain fire resistance at this temperature. When the temperature reached 1200 °C, the SiO_2 aerogel mortar had large cracks and apparent volume shrinkage after 0.5 h of fire-high temperature, indicating a loss of its fire-resistance ability.

3.6. Residual Mass Rate of SiO_2 Aerogel Mortar

Figure 5 shows the residual mass rate of SiO_2 aerogel mortar exposed to various fire temperatures and durations. All SiO_2 aerogel mortars experienced significant mass loss after 0.5 h of fire exposure, with a mass loss rate of about 10–11% in the 1000–1100 °C temperature range. Most of the mass loss was due to bound water evaporation, with a smaller portion attributed to C-S-H gel and $CaCO_3$ decomposition on the surface of SiO_2 aerogel mortar. However, at 1200 °C, the mass loss rate of SiO_2 aerogel mortar reached 20%. At this point, apparent volume shrinkage and large cracks were formed, and the high temperature penetrated from the outside to the inside, causing a rapid decomposition of hydration products and a sharp decline in mass.

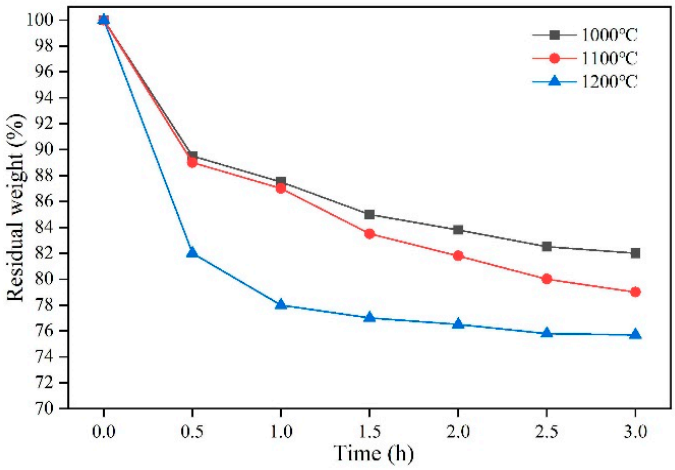

Figure 5. The residual mass rate of SiO_2 aerogel mortar after exposure to different fire temperatures and durations.

The mass of SiO_2 aerogel mortar specimens decreased gradually after exposure to high temperatures of 1000 and 1100 °C for 0.5 to 1 h, with a mass loss rate of about 2%, as the hydration products of cement continued to decompose with increasing fire duration. However, the mass loss rate of SiO_2 aerogel mortar specimens at 1200 °C was higher, reaching 4%, and severe cracking was observed. The mass loss rate of SiO_2 aerogel mortar increased significantly, reaching about 4%, indicating severe damage, when exposed to fire for 1 h to 1.5 h at temperatures of 1000 °C or 1100 °C. However, the mass loss rate stabilized when the fire temperature was 1200 °C, suggesting that the temperature penetration had nearly reached the center of the specimen. The mass loss rate of the SiO_2 aerogel mortar decreased again when the fire duration reached 1.5 h to 2 h, and the fire temperature was 1000 °C. However, this trend did not occur when the fire temperature was 1100 °C because

the aerogel structure collapsed, resulting in increased porosity and cracking after exposure to 1100 °C for 1.5 h. The mass loss rate of the SiO_2 aerogel mortar slowed down but still decreased when the fire duration was 2 h to 3 h, and the fire temperature was 1000 °C or 1100 °C. At 1200 °C, the mass of the SiO_2 aerogel mortar remained constant after 2–3 h of fire exposure, indicating complete burn-through and loss of fire resistance. The change rate suggested that the SiO_2 aerogel mortar had strong fire resistance at temperatures less than or equal to 1000 °C and could survive 3 h of fire exposure without being completely destroyed. At 1100 °C, its fire resistance was lower than that at 1000 °C, but it still required 3 h to be completely destroyed, indicating some degree of fire resistance at this temperature. At 1200 °C, the SiO_2 aerogel mortar was quickly destroyed and unsuitable for use at this temperature. The slowing trend of the mass loss rate with increasing fire duration also indicated that the heat transfer mode of the mortar during fire exposure was slow and layer-by-layer, demonstrating the high stability of the SiO_2 aerogel mortar under tunnel fire high-temperature conditions.

3.7. Residual Compressive Strength of SiO_2 Aerogel Mortar

Figure 6 shows the residual compressive strength of the SiO_2 aerogel mortar after exposure to different fire scenarios in a tunnel fire simulation. The results indicated that the residual compressive strength of the SiO_2 aerogel mortar decreased with the increase in fire temperature and duration. The strength reduction of the SiO_2 aerogel mortar was negligible, only 14%, at the fire temperature of 1000 °C for 0.5 h. It decreased steadily within 0.5–3 h, with a strength loss of 45.7% and a residual compressive strength of 1.9 MPa. At the fire temperature of 1100 °C, the strength reduction trend of the SiO_2 aerogel mortar from 0 to 2.5 h was similar to that at 1000 °C, remaining relatively stable with a residual compressive strength of 1.8 MPa, indicating good fire resistance at this point. However, the decrease rate accelerated from 2.5 to 3 h, and the strength decreased by 60% after 3 h, with a residual compressive strength of 1.4 MPa. It can be seen that the SiO_2 aerogel mortar experienced the most severe strength reduction, reaching 88.6%, after the fire temperature of 1200 °C for 3 h. After 0.5 h, the compressive strength of the specimen dropped sharply. At this time, large cracks emerged on the surface of the mortar, resulting in the volume shrinkage and the weakening of the bond force between the mortar and the aerogel particles. It was the main cause of the rapid decrease in its compressive strength.

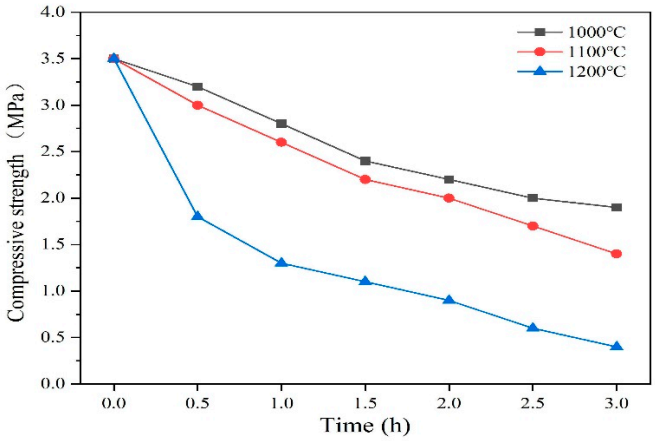

Figure 6. Residual compressive strength of SiO_2 aerogel mortar after exposure to different fire temperatures and durations.

3.8. SEM Analysis of SiO_2 Aerogel Mortar

The microstructure of the SiO_2 aerogel mortar exposed to different temperatures and durations of fire is shown in Figure 7. The degree of damage varied with the temperature and duration of the fire and increased as the fire lasted longer. The cement paste of the SiO_2 aerogel mortar became loose after exposure to 1000 and 1100 °C fires. However, when the

temperature reached 1200 °C, the microstructure of the SiO_2 aerogel mortar became dense after the fire, which was consistent with the macroscopic changes. Notably, at 1000 °C, the cement matrix was mainly affected, while the aerogel particles remained relatively intact, as shown in Figure 2. At 1100 °C, the damage of the SiO_2 aerogel mortar consisted of two parts: rapid decomposition of hydration products and shrinkage of the aerogel. When the fire lasted for 0.5–1 h, the damage rate was slow, and no obvious shrinkage of aerogel particles was observed. After 2 h, the aerogel particles were almost completely shrunk. At 1200 °C, the SiO_2 aerogel mortar suffered severe damage after 0.5 h of exposure, and the degree of damage did not change much with time. These trends indicate that the SiO_2 aerogel mortar had high fire resistance at 1000 °C. At 1100 °C, its fire resistance decreased but was still considerable. At 1200 °C, the SiO_2 aerogel mortar had almost no fire resistance.

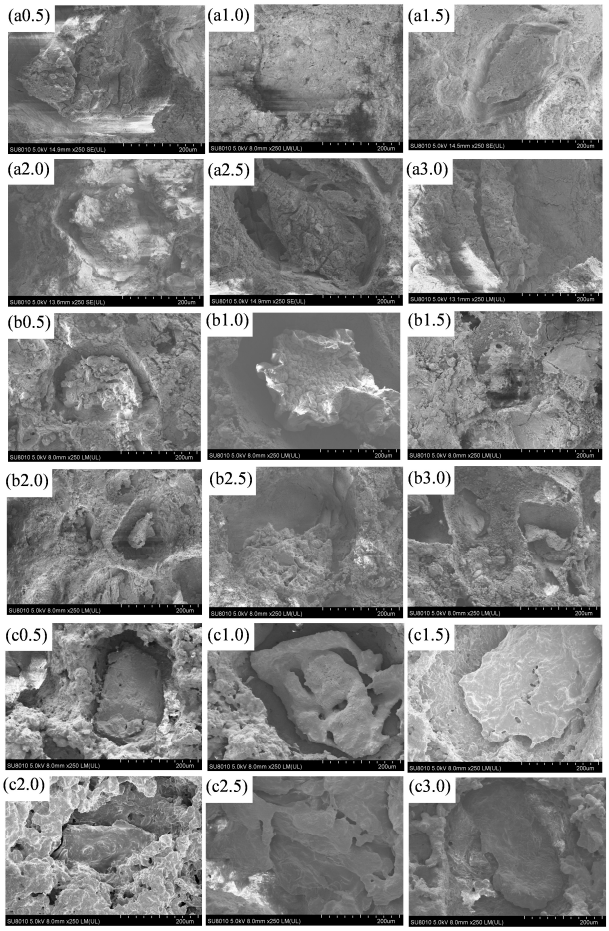

Figure 7. SEM images of SiO_2 aerogel mortar after exposure to different fire temperatures and durations: (**a**) 1000 °C; (**b**) 1100 °C; (**c**) 1200 °C.

3.9. XRD Analysis of SiO_2 Aerogel Mortar

Figure 8 shows the XRD results of SiO_2 aerogel mortar subjected to different fire temperatures and durations. The diffraction peak labeled 1 corresponds to the $CaCO_3$ crystal [45], the peak labeled 2 corresponds to the SiO_2 crystal [40], the peak labeled 3 corresponds to the Ca_2SiO_4 crystal [46,47], and the peak labeled 4 corresponds to the $Ca_2Al_2SiO_7$ crystal [48].

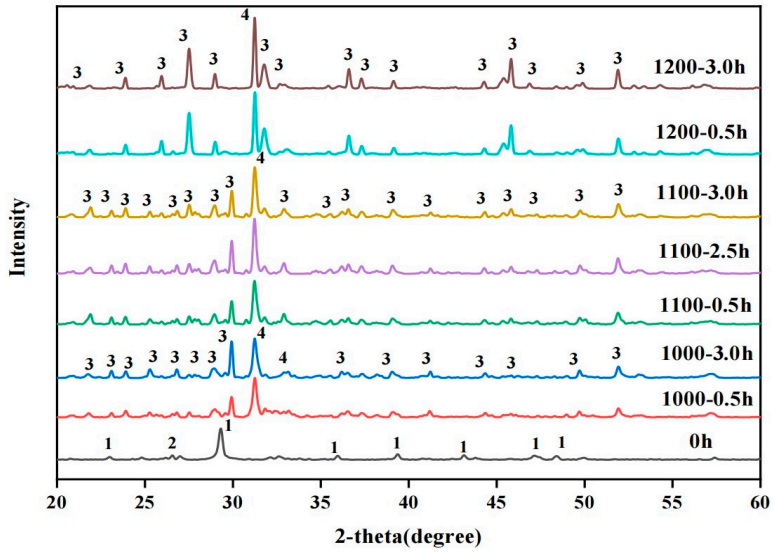

Figure 8. XRD patterns of SiO_2 aerogel mortar after exposure to different fire temperatures and durations.

The experimental temperature ranged from 1000 to 1200 °C. The XRD results revealed that C-S-H gel and $CaCO_3$ were the main components decomposed at high temperatures. The XRD patterns at different temperatures revealed that the crystallinity of the crystals enhanced as the fire temperature increased, indicating that the material suffered more damage. Particularly at 1200 °C, the crystallinity of the SiO_2 aerogel mortar was much higher than that at other temperatures, which accounted for why the SiO_2 aerogel mortar contracted sharply and hardened at 1200 °C. Moreover, the crystallinity of the SiO_2 aerogel mortar increased with increasing fire duration at 1000 and 1100 °C. While at 1200 °C, the fire duration of 0.5 and 3 h had no significant influence on its crystallinity, suggesting that the reaction was completed very quickly at this temperature within 0.5 h, further demonstrating its poor fire resistance at 1200 °C, which was in agreement with other test results. When the temperature was 1000 °C, the crystallinity of $Ca_2Al_2SiO_7$ and Ca_2SiO_4 crystals generated by the SiO_2 aerogel mortar after high-temperature decomposition continued to increase until the fire ended after 3 h. At 1100 °C, the decomposition of the SiO_2 aerogel mortar finished at 2.5 h, which indicated its potential application under tunnel fires at 1100 °C.

4. Conclusions

This paper presented a novel fireproof mortar prepared by replacing the conventional aggregate with a SiO_2 aerogel and investigated its damage mechanisms under different fire temperatures and durations in a tunnel fire simulation. The main conclusions are as follows:

(1) The critical temperature and critical time of SiO_2 aerogel particles from amorphous to crystalline structure were about 1100 °C and 1.5 h, respectively.

(2) The SiO_2 aerogel mortar developed in this study exhibited low thermal conductivity and high mechanical properties. The compressive strength, bond strength, dry density, water resistance, moisture resistance, and freeze–thaw resistance of the SiO_2 aerogel mortar met the requirements for its use as a fireproof coating.

(3) The damage degree of the SiO_2 aerogel mortar increased with the increase in fire temperature and duration from both macroscopic and microscopic perspectives. It exhibited superior fire resistance and maintained volume stability when exposed to temperatures of 1000 °C and 1100 °C. The damage degree under the fire temperature of 1200 °C was much higher than that under 1000 and 1100 °C.

(4) Compared with the performance of the SiO_2 aerogel mortar at fire temperature of 1200 °C, its mass and compressive strength decreased smoothly at fire temperatures of

1000 and 1100 °C. After being exposed to fire temperature of 1100 °C for 2.5 h, the residual mass ratio and residual compressive strength were 81% and 1.8 MPa, respectively.

(5) The test results indicated that the SiO_2 aerogel mortar can be used as a fireproofing coating, capable of withstanding tunnel fires at 1100 °C for 2.5 h.

Author Contributions: Conceptualization, H.C. and P.Z.; methodology, H.C. and P.Z.; software, H.C.; validation, X.Y. and X.X.; formal analysis, P.Z.; investigation, H.C., P.Z. and X.X.; data curation, X.W.; writing—original draft preparation, H.C.; writing—review and editing, P.Z. and X.Y.; visualization, H.C.; supervision, P.Z. and X.W.; project administration, P.Z.; funding acquisition, H.C., P.Z. and X.W. All authors have read and agreed to the published version of the manuscript.

Funding: This research was funded by the National Natural Science Foundation of China (52078068); Postgraduate Research & Practice Innovation Program of Jiangsu Province (SJCX22-1370).

Institutional Review Board Statement: Not applicable.

Informed Consent Statement: Not applicable.

Data Availability Statement: The data used to support the findings of this study are available from the corresponding author upon request.

Conflicts of Interest: The authors declare no conflict of interest.

References

1. Santos-Reyes, J.; Beard, A.N. An analysis of the emergency response system of the 1996 Channel tunnel fire. *Tunn. Undergr. Space Technol.* **2017**, *65*, 121–139. [CrossRef]
2. Guo, C.; Zhang, T.; Guo, Q.; Yu, T.; Fang, Z.; Yan, Z. Full-scale experimental study on fire characteristics induced by double fire sources in a two-lane road tunnel. *Tunn. Undergr. Space Technol.* **2023**, *131*, 104768. [CrossRef]
3. Chen, H.; Liu, T.; You, X.; Yuan, D.; Ping, Y.; Zhang, Q. Experimental investigation on fire damage to staggered segmental lining of shield tunnel. *Tunn. Undergr. Space Technol.* **2023**, *141*, 105359. [CrossRef]
4. Ingason, H. Design fire curves for tunnels. *Fire Saf. J.* **2009**, *44*, 259–265. [CrossRef]
5. de Silva, D.; Andreini, M.; Bilotta, A.; De Rosa, G.; La Mendola, S.; Nigro, E.; Rios, O. Structural safety assessment of concrete tunnel lining subjected to fire. *Fire Saf. J.* **2022**, *134*, 103697. [CrossRef]
6. Lai, J.; Qiu, J.; Fan, H.; Chen, J.; Xie, Y. Freeze-proof method and test verification of a cold region tunnel employing electric heat tracing. *Tunn. Undergr. Space Technol.* **2016**, *60*, 56–65. [CrossRef]
7. Li, Y.Z.; Ingason, H. Overview of research on fire safety in underground road and railway tunnels. *Tunn. Undergr. Space Technol.* **2018**, *81*, 568–589. [CrossRef]
8. Qiu, J.; Yang, T.; Wang, X.; Wang, L.; Zhang, G. Review of the flame retardancy on highway tunnel asphalt pavement. *Constr. Build. Mater.* **2019**, *195*, 468–482. [CrossRef]
9. Guo, X.; Pan, X.; Zhang, L.; Wang, Z.; Hua, M.; Jiang, J. Comparative study on ventilation and smoke extraction systems of different super-long river-crossing subway tunnels under fire scenarios. *Tunn. Undergr. Space Technol.* **2021**, *113*, 103849. [CrossRef]
10. Wang, F.; Wang, M.; Huo, J. The effects of the passive fire protection layer on the behavior of concrete tunnel linings: A field fire testing study. *Tunn. Undergr. Space Technol.* **2017**, *69*, 162–170. [CrossRef]
11. Peng, G.; Niu, X.; Shang, Y.; Zhang, D.; Chen, X.; Ding, H. Combined curing as a novel approach to improve resistance of ultra-high performance concrete to explosive spalling under high temperature and its mechanical properties. *Cem. Concr. Res.* **2018**, *109*, 147–158. [CrossRef]
12. Lura, P.; Terrasi, G.P. Reduction of fire spalling in high-performance concrete by means of superabsorbent polymers and polypropylene fibers. *Cem. Concr. Compos.* **2014**, *49*, 36–42. [CrossRef]
13. Liang, X.; Wu, C.; Su, Y.; Chen, Z.; Li, Z. Development of ultra-high performance concrete with high fire resistance. *Constr. Build. Mater.* **2018**, *179*, 400–412. [CrossRef]
14. Netinger Grubeša, I.; Marković, B.; Gojević, A.; Brdarić, J. Effect of hemp fibers on fire resistance of concrete. *Constr. Build. Mater.* **2018**, *184*, 473–484. [CrossRef]
15. Bezgin, N.Ö. An experimental evaluation to determine the required thickness of passive fire protection layer for high strength concrete tunnel segments. *Constr. Build. Mater.* **2015**, *95*, 279–286. [CrossRef]
16. Koksal, F.; Coşar, K.; Dener, M.; Benli, A.; Gencel, O. Insulating and fire-resistance performance of calcium aluminate cement based lightweight mortars. *Constr. Build. Mater.* **2023**, *362*, 129759. [CrossRef]
17. Huang, W.; Wang, Y.; Zhang, Y.; Zheng, W. Experimental study of high-temperature resistance of alkali-activated slag crushed aggregate mortar. *J. Mater. Res. Technol.* **2023**, *23*, 3961–3973. [CrossRef]
18. Ding, C.; Xue, K.; Cui, H.; Xu, Z.; Yang, H.; Bao, X.; Yi, G. Research on fire resistance of silica fume insulation mortar. *J. Mater. Res. Technol.* **2023**, *25*, 1273–1288. [CrossRef]

19. Krivenko, P.V.; Guzii, S.G.; Bodnarova, L.; Valek, J.; Hela, R.; Zach, J. Effect of thickness of the intumescent alkali aluminosilicate coating on temperature distribution in reinforced concrete. *J. Build. Eng.* **2016**, *8*, 14–19. [CrossRef]
20. Soleimani Dorcheh, A.; Abbasi, M.H. Silica aerogel; synthesis, properties and characterization. *J. Mater. Process. Technol.* **2008**, *199*, 10–26. [CrossRef]
21. Lamy-Mendes, A.; Pontinha, A.D.R.; Alves, P.; Santos, P.; Durães, L. Progress in silica aerogel-containing materials for buildings' thermal insulation. *Constr. Build. Mater.* **2021**, *286*, 122815. [CrossRef]
22. Ihara, T.; Grynning, S.; Gao, T.; Gustavsen, A.; Jelle, B.P. Impact of convection on thermal performance of aerogel granulate glazing systems. *Energy Build.* **2015**, *88*, 165–173. [CrossRef]
23. Yang, J.; Wu, H.; Xu, X.; Huang, G.; Xu, T.; Guo, S.; Liang, Y. Numerical and experimental study on the thermal performance of aerogel insulating panels for building energy efficiency. *Renew. Energy* **2019**, *138*, 445–457. [CrossRef]
24. Wang, C.; Liang, W.; Yang, Y.; Liu, F.; Sun, H.; Zhu, Z.; Li, A. Biomass carbon aerogels based shape-stable phase change composites with high light-to-thermal efficiency for energy storage. *Renew. Energy* **2020**, *153*, 182–192. [CrossRef]
25. Zhang, Z.; Li, B.; Wang, Z.; Liu, W.; Liu, X. Development of reduced thermal conductivity ductile cement-based composite material by using silica aerogel and silane. *J. Build. Eng.* **2023**, *65*, 105698. [CrossRef]
26. Lu, J.; Jiang, J.; Lu, Z.; Li, J.; Niu, Y.; Yang, Y. Pore structure and hardened properties of aerogel/cement composites based on nanosilica and surface modification. *Constr. Build. Mater.* **2020**, *245*, 118434. [CrossRef]
27. Sonnick, S.; Meier, M.; Ross-Jones, J.; Erlbeck, L.; Medina, I.; Nirschl, H.; Rädle, M. Correlation of pore size distribution with thermal conductivity of precipitated silica and experimental determination of the coupling effect. *Appl. Therm. Eng.* **2019**, *150*, 1037–1045. [CrossRef]
28. Huang, D.; Guo, C.; Zhang, M.; Shi, L. Characteristics of nanoporous silica aerogel under high temperature from 950 °C to 1200 °C. *Mater. Des.* **2017**, *129*, 82–90. [CrossRef]
29. Lei, Y.; Chen, X.; Song, H.; Hu, Z.; Cao, B. The influence of thermal treatment on the microstructure and thermal insulation performance of silica aerogels. *J. Non-Cryst. Solids* **2017**, *470*, 178–183. [CrossRef]
30. Cai, H.; Jiang, Y.; Feng, J.; Chen, Q.; Zhang, S.; Li, L.; Feng, J. Nanostructure evolution of silica aerogels under rapid heating from 600 °C to 1300 °C via in-situ TEM observation. *Ceram. Int.* **2020**, *46*, 12489–12498. [CrossRef]
31. *GB/T20473-2021*; Dry-Mixed Thermal Insulating Mortar for Buildings. Standardization Administration of China: Beijing, China, 2021.
32. *GB28375-2012*; Fireproof Coatings for Concrete Structure. Standardization Administration of China: Beijing, China, 2012.
33. *JGJ/70-2009*; Standard for Test Method of Basic Properties of Construction Mortar. Standardization Administration of China: Beijing, China, 2009.
34. *GB/T10294-2008*; Thermal Insulation-Determination of Steady-State Thermal Resistance and Related Properties-Heat Flow Meter Apparatus. Standardization Administration of China: Beijing, China, 2008.
35. Koebel, M.; Rigacci, A.; Achard, P. Aerogel-based thermal superinsulation: An overview. *J. Sol-Gel Sci. Technol.* **2012**, *63*, 315–339. [CrossRef]
36. Zhang, X.; Jiang, Y.; Xu, N.; Liu, H.; Wu, N.; Han, C.; Wang, B.; Wang, Y. Thermal stable, fire-resistant and high strength SiBNO fiber/SiO_2 aerogel composites with excellent thermal insulation and wave-transparent performances. *Mater. Today Commun.* **2022**, *33*, 104261. [CrossRef]
37. Pan, Y.; He, S.; Gong, L.; Cheng, X.; Li, C.; Li, Z.; Liu, Z.; Zhang, H. Low thermal-conductivity and high thermal stable silica aerogel based on MTMS/Water-glass co-precursor prepared by freeze drying. *Mater. Des.* **2017**, *113*, 246–253. [CrossRef]
38. Ahmad, S.; Ahmad, S.; Sheikh, J.N. Silica centered aerogels as advanced functional material and their applications: A review. *J. Non-Cryst. Solids* **2023**, *611*, 122322. [CrossRef]
39. Poletto, M.; Ornaghi, H.; Zattera, A. Native Cellulose: Structure, Characterization and Thermal Properties. *Materials* **2014**, *7*, 6105–6119. [CrossRef]
40. Hu, Y.; Xiao, Z.; Wang, H.; Ye, C.; Wu, Y.; Xu, S. Fabrication and characterization of porous $CaSiO_3$ ceramics. *Ceram. Int.* **2019**, *45*, 3710–3714. [CrossRef]
41. Du, B.; Hong, C.; Wang, A.; Zhou, S.; Qu, Q.; Zhou, S.; Zhang, X. Preparation and structural evolution of SiOC preceramic aerogel during high-temperature treatment. *Ceram. Int.* **2018**, *44*, 563–570. [CrossRef]
42. Zhu, P.; Brunner, S.; Zhao, S.; Griffa, M.; Leemann, A.; Toropovs, N.; Malekos, A.; Koebel, M.M.; Lura, P. Study of physical properties and microstructure of aerogel-cement mortars for improving the fire safety of high-performance concrete linings in tunnels. *Cem. Concr. Compos.* **2019**, *104*, 103414. [CrossRef]
43. Chousidis, N.; Constantinides, G. Fire endurance and corrosion resistance of nano-modified cement mortars exposed to elevated temperatures. *Ceram. Int.* **2023**, *49*, 19182–19193. [CrossRef]
44. Kanagaraj, B.; Anand, N.; Cashell, K.A.; Andrushia, A.D. Post-fire behaviour of concrete containing nano-materials as a cement replacement material. *Case Stud. Constr. Mater.* **2023**, *18*, e2171. [CrossRef]
45. Liu, H.; Zhao, Y.; Peng, C.; Song, S.; Lopez-Valdivieso, A. Lime mortars—The role of carboxymethyl cellulose on the crystallization of calcium carbonate. *Constr. Build. Mater.* **2018**, *168*, 169–177. [CrossRef]
46. Ahn, Y.B.; Jang, J.G.; Lee, H.K. Mechanical properties of lightweight concrete made with coal ashes after exposure to elevated temperatures. *Cem. Concr. Compos.* **2016**, *72*, 27–38. [CrossRef]

47. Link, T.; Bellmann, F.; Ludwig, H.M.; Haha, M.B. Reactivity and phase composition of Ca2SiO4 binders made by annealing of alpha-dicalcium silicate hydrate. *Cem. Concr. Res.* **2015**, *67*, 131–137. [CrossRef]
48. Pan, Z.; Tao, Z.; Murphy, T.; Wuhrer, R. High temperature performance of mortars containing fine glass powders. *J. Clean. Prod.* **2017**, *162*, 16–26. [CrossRef]